



HAL
open science

High frequency characterization of a vertical electro-absorption modulator for data communications

Ludovic Marigo-Lombart, Christophe Viallon, Alexandre Rumeau, Olivier Gauthier-Lafaye, Antoine Monmayrant, Hugo Thienpont, Krassimir Panajotov, Guilhem Almuneau

► To cite this version:

Ludovic Marigo-Lombart, Christophe Viallon, Alexandre Rumeau, Olivier Gauthier-Lafaye, Antoine Monmayrant, et al.. High frequency characterization of a vertical electro-absorption modulator for data communications. 2018 International Topical Meeting on Microwave Photonics (MWP), IEEE, Oct 2018, Toulouse, France. hal-01980197

HAL Id: hal-01980197

<https://laas.hal.science/hal-01980197>

Submitted on 14 Jan 2019

HAL is a multi-disciplinary open access archive for the deposit and dissemination of scientific research documents, whether they are published or not. The documents may come from teaching and research institutions in France or abroad, or from public or private research centers.

L'archive ouverte pluridisciplinaire **HAL**, est destinée au dépôt et à la diffusion de documents scientifiques de niveau recherche, publiés ou non, émanant des établissements d'enseignement et de recherche français ou étrangers, des laboratoires publics ou privés.

High frequency characterization of a vertical electro-absorption modulator for data communications

L. Marigo-Lombart^{1,2}, C. Viallon¹, A. Rumeau¹, O. Gauthier-Lafaye¹, A. Monmayrant¹, H. Thienpont², K. Panajotov² and G. Almuneau¹

¹ LAAS-CNRS, Université de Toulouse, CNRS, Toulouse, France

² Department of Applied Physics and Photonics (TW-TONA), Vrije Universiteit Brussel, Pleinlaan 2, B-1050 Brussels, Belgium
lmarigol@laas.fr - kpanajot@b-phot.org - almuneau@laas.fr

Abstract—This paper describes the high-frequency characterizations of a vertical electro-absorption modulator (EAM) to ensure its monolithic integration onto a VCSEL for data communications. Splitting the emitting and the modulating part in such devices is an attractive approach compared to directly current-modulated VCSEL since it releases the intrinsic limitations due to carriers dynamics in such VCSEL device. It is, in this aim, utmost to thoroughly characterize and understand the properties and performances of the vertically integrated EAM under high frequency operation, as it will be decisive for the application of EAM-VCSEL to very high data-rate communications. EAM measurements, presented up to 40 GHz, require a precise control of the optical fiber coupling and a precise evaluation of the injection losses over the full frequency range.

Index Terms—Modulator, Electro-Absorption, VCSEL, high-frequency

I. INTRODUCTION

Nowadays, Vertical-Cavity Surface-Emitting Lasers (VCSELs) raise great awareness for their applications in numerous markets from the optical mouse to the 3D sensing, but primarily to extend the capacity of optical communications within datacenters, with a great concern on power consumption limitation. Indeed, VCSELs bring many advantages compared to edge emitters such as high density integration capabilities and easy coupling in optical fiber, making them ideal as light sources for very high frequency and high capacity optical datalinks. The direct modulation approach has been recently extensively developed and improved through many design strategies, but the physical limitation due to carriers dynamics poses a physical barrier. Therefore it is necessary to move forward to another solution to overcome this fundamental issue. For example, splitting of the emitting/gain and the modulating sections has already been proposed by several groups by combining an electro-optic modulator and a VCSEL, laterally [1] or within a vertical integration scheme. In this last configuration two solutions are possible. The first one is by modulating the refractive index of the top mirror (Distributed Bragg Reflector, DBR), and so the reflective spectrum via an electric field [2]. In that case both cavities

are coupled which allows very high bandwidth at the expense of an important chirp and a low transmission data rate. The second one, based on the absorption modulation by quantum-confined Stark effect, in which both optical cavities are weakly coupled, has already reached high frequency bandwidth with regulated temperature [3]. In this project, we focus on this last approach with the vertical integration of an electro-absorption modulator (EAM) onto a CW powered VCSEL. The high-frequency modulation performance relies then only on the modulator itself, independently of the VCSEL light source. The effectiveness of this integrated EAM-VCSEL scheme has already been demonstrated by static measurements with achievable modulation depth of 40 % at a 4V reverse bias [4].

In this paper, we focus on the characterization of the high-frequency electro-optic response of the modulator, by measuring its top reflectivity by fiber butt-coupling and using an external laser source. After a short description of the EAM structure and functioning, two measurement setups intended for bandwidth characterization are compared: one with a vector network analyzer (VNA) and the other one with a frequency synthesizer and a spectrum analyzer. For higher measurement accuracy, specially at high frequencies, the implemented InGaAs photodiode response has been measured by heterodyne beat at 850 nm and 1550 nm to be compared with the supplier data. Results are finally presented and described while considering all the electrical losses across the injection chain and including the photodiode response.

II. DEVICES DESCRIPTION

The EAM is composed of a multiple quantum wells cavity sandwiched between two DBR to increase the absorption in the active region as described in [4]. The maximum modulation depth is obtained at 838 nm when a reverse bias, for doped DBR, of 4 V is applied to modify the band diagram of the structure. A very fast variation of the EAM absorption can be obtained by adding a RF small-signal to the voltage bias, making this EAM a voltage-driven device. Due to the non-doped cavity region (around 500 nm) the EAM presents a high

impedance which drops when the frequency is increased. The schematic of the global EAM-VCSEL device is represented in Fig. 1. We processed the sample for high-frequency operation and thus planarized it with BCB to decrease the parasitics capacitance and used a microstrip line access for the radio-frequency (RF) signal injection.

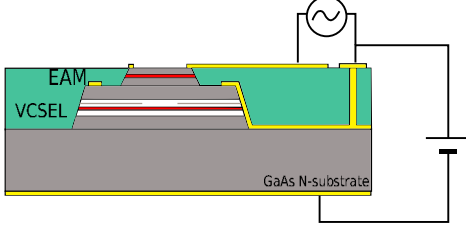


Fig. 1. Schematic of the EAM-VCSEL device powering.

With the characterization setups described below, the proper operation of the modulator is verified for different voltage values and illuminating wavelengths.

III. DEVICE CHARACTERIZATION

A dedicated electro-optical characterization setup has been developed to vertically inject and detect light through a single-mode Y fiber coupler on the modulator top surface. The incident monochromatic light is supplied by a tunable laser source (TLS) and the reflected EAM-modulated signal is measured using a high-speed photodiode as seen in red in Fig. 2. The TLS is a Superlum BS-840-1 (820 - 840 nm, linewidth = 0.06 nm) and the employed InGaAs Discovery DSC20H-39 photodiode displays a cut-off frequency of 32 GHz at 1550 nm. The RF injection is either carried out by a VNA source or by a distinct RF synthesizer as described in the next subsections. Finally, the -3 dB cut-off frequency of the device is obtained by normalizing the photodetected EAM response under RF voltage excitation with the response obtained at the lowest frequency voltage.

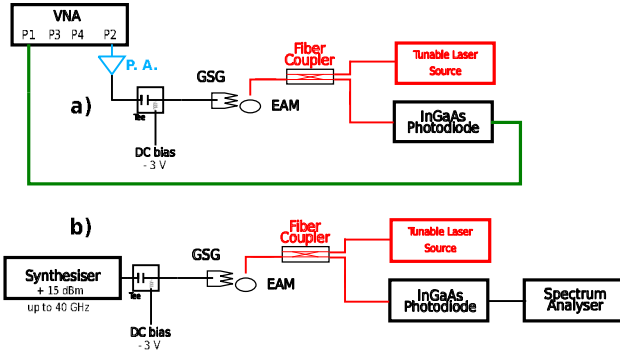


Fig. 2. Schematics of the electro-optic characterization of the EAM with a VNA (a) and with a synthesiser (b).

A. VNA implementation

The first implementation is displayed in Fig. 2a. A VNA Agilent PNA-X 67 GHz is used to extract the EAM response. Since the signal retrieved by the photodiode is too low due to several cumulative factors (EAM reflectivity, fiber misalignment and photodiode responsivity in the near-infrared range),

a power amplifier (PA) featuring a maximum output power of $+24$ dBm has been inserted between VNA and EAM RF input. The port 2 is connected to the EAM through this PA, a bias Tee, a coaxial K-band cable and a Cascade Infinity 40 GHz coplanar on-wafer RF probe. Any change in EAM reflectivity is measured by the photodiode and sent to the port 1. The EAM bandwidth is extracted from the measured transmission parameter S_{12} and the PA-limited 10 MHz - 18 GHz frequency range is covered in one sweep by the VNA.

1) *Preliminary results:* The first set of measurements is plotted in Fig. 3. As we can see in red, green and black, any modification in the EAM DC voltage bias and TLS wavelength changes the S_{12} magnitude observed on the VNA. This clearly indicates that a modulation effect takes place within the EAM section, thus demonstrating the effective electro-absorption modulation at such frequencies. It is interesting to note that the slope observed between 1 GHz and 18 GHz remains unchanged whatever the voltage and wavelength values.

Jointly, we have measured the electrical losses in the "PA + bias tee + Cable" response, in black at the top in Fig. 3. This result confirms that the slope seen in all S_{12} curves is strongly related to the RF signal injection losses. If these losses are subtracted from the raw transmission measurements, a very flat response from the EAM is obtained all over the 1-18 GHz frequency range (blue curve).

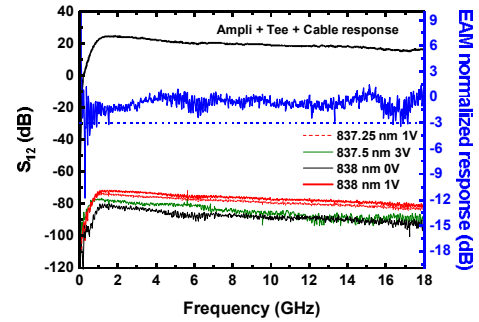


Fig. 3. EAM response (S_{12}) measured by the VNA-based test setup.

2) *Limitations:* This result shows that we are especially limited by the bandwidth of the PA and by the losses within the test bench between VNA and EAM device. One solution to overcome these limitations should be to change the available power set at the input of the EAM for each frequency point. Unfortunately such an option is usually not available in VNAs.

B. RF synthesizer and spectrum analyzer

In this subsection we present the second measurement setup we have developed, which mainly consists in replacing the VNA by an RF synthesizer (Anritsu MG 3694B) coupled with a spectrum analyzer (Fieldfox N9951 A from Keysight) at the photodiode output. This second version of the measurement bench is shown in Fig. 2b. The most important improvements brought by this new configuration are the nearly constant power delivered by this RF synthesizer all over the 40 GHz bandwidth as well as the pre-amplifier integrated within the spectrum analyzer which increases the electrical signal level issued by the photodiode.

1) *Calibration*: We have gained a valuable experience with previous measurements and we now know that the losses calibration is the key point of the setup. Firstly, the output power of the synthesizer, set to a value of +15 dBm, is verified by using a powermeter (Anritsu ML 2437A). This measurement value, plotted in Fig. 4 (black curve), presents a delta of 0.9 dB in the 1 - 40 GHz frequency range. The insertion of the bias tee and cable system lowers the available power by a maximum value of 3.5 dB in the same frequency range (blue curve). These losses have to be compensated to extract a more realistic EAM response.

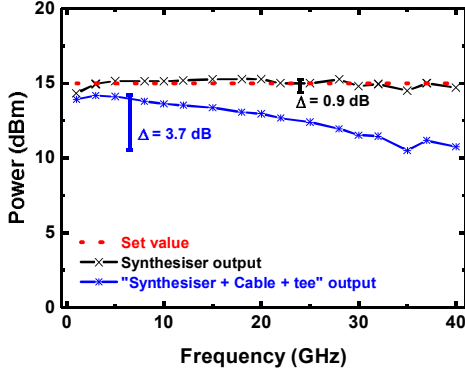


Fig. 4. Power calibration of the RF synthesiser set to +15 dBm alone (black curve) and with the system "bias tee + cable" (blue curve).

2) *Preliminary results*: Previous results are used to adjust the power delivered by the RF synthesizer so as to provide a constant value of +15 dBm at the input of the RF probe connected to EAM pads. Several measurements carried on various EAM (diameters from 18 to 27 μm) integrated alones or onto VCSELs have revealed that the VCSEL cavity has no influence on EAM response. But whatever the tested configuration, a constant -5 dB/dec slope is still observed all over the measured frequency range. However, since the cut-off frequency is linked to the capacitance of the device and thus to its mesa diameter, we should have observed different slopes for each tested diameter. The absence of difference clearly indicates that this observed slope cannot be traced to the low-pass nature of EAM devices. RF probes, EAM pad and microstrip access line contribution to the overall insertion losses have been neglected since it does not exceed 1 dB at 40 GHz it cannot explain this -5 dB/dec slope too.

3) *Losses compensation*: As already stated before, the EAM RF input presents a very high impedance. All the measurement chain starting from RF source up to the RF probe tips is loaded by an impedance approaching an open circuit at the lowest frequencies. This impedance decreases with increasing frequencies but still remains much larger than 50Ω at 40 GHz. The determination of the EAM response based on the measurement of the available power cannot be satisfactory due to this frequency varying mismatch. Since the EAM is fundamentally a voltage driven device, a more natural approach is to use the applied voltage magnitude to recover its frequency response. This voltage can be assessed

from the knowledge of the available power from RF source, the scattering parameters of the test setup, and the EAM impedance. This problem is illustrated in Fig.5. The RF source is modeled by its Thevenin generator V_g followed by a serie resistance $R_g = 50 \Omega = R_0$. The test setup comprising the bias tee, the cable and the RF probe is depicted by the two-port network and its scattering matrix. Finally, V_L is the voltage across the input impedance of the EAM.

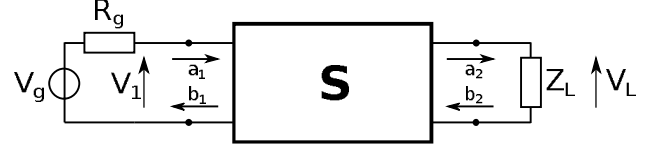


Fig. 5. Schematic of the RF signal injection from RF source to EAM input.

Let Γ_L , Γ_g and Γ_{in} be the reflection coefficients displayed by the EAM, the RF source and the two-port network input, respectively.

$$\Gamma_L = \frac{Z_L - R_0}{Z_L + R_0} \quad (1)$$

$$\Gamma_g = \frac{R_g - R_0}{R_g + R_0} \quad (2)$$

$$\Gamma_{in} = S_{11} + \frac{S_{12}S_{21}\Gamma_L}{1 - S_{22}\Gamma_L} \quad (3)$$

The signal flow graph technique [6] is used to find the relationship between voltage V_L and V_g , using the two-port scattering parameters, Γ_L , Γ_g and Γ_{in} :

$$V_L = \frac{S_{21}}{2} \cdot \frac{1 + \Gamma_L}{1 - \Gamma_L S_{22}} \cdot \frac{1 - \Gamma_g}{1 - \Gamma_g \Gamma_{in}} \cdot V_g \quad (4)$$

V_g is deduced from the available power measured across R_0 which is also the input impedance of the powermeter:

$$P_{disp} = \frac{1}{2} \cdot \frac{|V_g|^2}{4R_0} \implies |V_g| = \sqrt{8R_0 P_{disp}} \quad (5)$$

In practice, the complete two-port scattering matrix cannot be measured easily because of the different nature of input (SMA cable) and output (RF probe tips) terminals of this box. However, the matrix is symmetric and $S_{12} = S_{21}$. S_{ij} parameters are extracted from measurements carried out using a SHORT or OPEN circuit at RF probe ends while $S_{11} = S_{22}$ are assumed to be zero, which is not too far from reality. Using this assumption, $|V_L|$ becomes

$$|V_L| = |S_{21}| \cdot |1 + \Gamma_L| \cdot \sqrt{2R_0 P_{disp}} \quad (6)$$

With this last equation, we are now able to link the EAM voltage to the available power measured at the RF source output. The idea is now to calculate the power we need to set so as to maintain a constant voltage at EAM pads all over the studied frequency range.

C. Photodiode characterization and results

The last thing to validate in the electro-optical setup is the photodiode frequency response at 850 nm. In previous measurements we dealt with the supplier data given at 1550 nm but the response may be different at 850 nm. Hence, the photodiode response has been measured by using an

heterodyne beating technique at 850 nm and also at 1550 nm to compare the results with the supplier data.

At 1550 nm we used an InGaAs DFB at 1537.2 nm regulated by an IXL Lighthwave LDC-3722 B at 22.9 °C biased at 70.1 mA to deliver -3 dBm in the photodiode under test. The used tunable laser is a Santec TSL-510 and is conveyed to the photodiode through a polarization maintaining coupler. At 850 nm, the stationary laser is a homemade laser formed with a LED and a Cavity Resonator Integrated Grating Filter (CRIGF) [5] which filters a precise wavelength, here 854 nm. The LED is biased at 52 mA, 1.7 V and is maintained at 20 °C to maintain single mode operation. The other laser is a Vantage TLB7100 from Newfocus. For both measurements, the photodiode response is sent in a Rohde & Schwarz spectrum analyzer and is extracted from 20 Hz up to 40 GHz. For each wavelength we acquired 10 spectra and did an average to decrease the uncertainty due to the vibration or air flow in the room.

The results are presented in Fig. 6. At 1550 nm, the same response than supplier data is obtained which makes us confident with the result displayed at 850 nm. As we can see, the photodiode response at 850 nm is really different from the one at 1550nm. This new characteristic is used to improve the measurement precision of the modulator cut-off frequency.

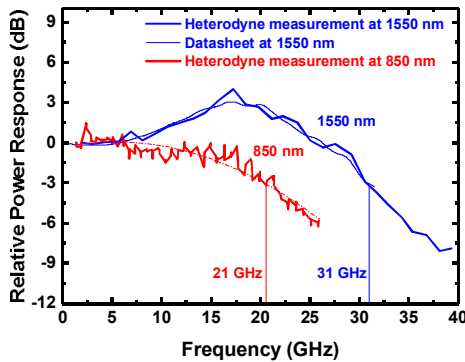


Fig. 6. Characterization of the InGaAs photodiode at 1550 nm (blue) and 850 nm (red).

We then measured a $27 \mu\text{m}$ -diameter EAM at 838 nm with a bias offset of 3 V and a RF signal amplitude of 0.8 V at the EAM pad plane. The signal detected by the InGaAs photodiode is presented in Fig. 7. The effects of the photodiode responses compensation are displayed. As shown in Fig. 7, the cut-off frequency of the EAM is evaluated up to more than 23 GHz, instead of around 15 GHz when considering the photodiode supplier characteristics at 1550 nm. The EAM high frequency response could not be further characterized above 23 GHz, since the photodiode responsivity drops drastically.

IV. CONCLUSION

In this paper we present different setups for the electro-optical characterization of a vertical EAM. First, with a VNA but this characterization turns out to be limited by the frequency range of the power amplifier used to measure the modulated signal. And secondly, we proposed an original setup

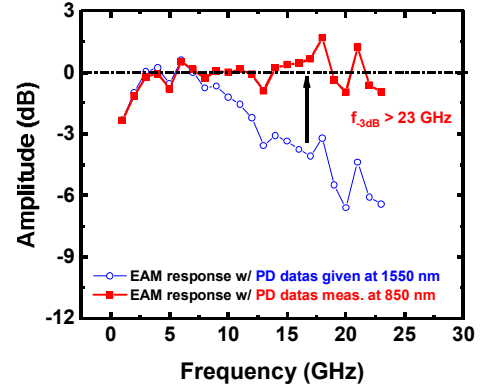


Fig. 7. High frequency characterization of the $27 \mu\text{m}$ -EAM.

involving a RF synthesizer along with a spectrum analyzer to extend the measurement frequency range up to 40 GHz. This setup finally appears limited by the responsivity of the photodiode. Thanks to these improvements, we are able to measure a cut-off frequency above 23 GHz for this vertical GaAs-based asymmetric Fabry-Perot electro-absorption modulator. This result can be compared to the 20 GHz modulation demonstrated in [3] which employs a similar approach. To our knowledge, this result is the best achieved modulation bandwidth for this type of architecture, compatible with the monolithic integration onto a VCSEL source.

ACKNOWLEDGMENT

The authors gratefully acknowledge the technological support of RENATECH (French Network of Technology Platforms) within LAAS-CNRS cleanroom infrastructure and the financial support by the Methusalem foundation, Belgium.

REFERENCES

- [1] X. Gu, M. Nakahama, A. Matsutani, M. Ahmed, A. Bakry and F. Koyama, "850 nm transverse-coupled-cavity vertical-cavity surface-emitting laser with direct modulation bandwidth of over 30 GHz", *Appl. Phys. Expr.* 8, 082702, 2015
- [2] T. D. Germann, A. Strittmatter, A. Mutig, A. M. Nadtochiv, J. A. Lott, S. A. Blokhin, et al., "Monolithic electro-optically modulated vertical cavity surface emitting laser with 10 Gb/s open-eye operation", *Phys. Status Solidi C* 7, No. 10, 2552-2554, 2010
- [3] J. van Eijsden, M. Yakimov, V. Tokranov, M. Varanasi, O. Romyantsev, E. M. Mohammed, et al. "High Frequency Resonance-Free Loss Modulation in a Duo-Cavity VCSEL", *Proc. of SPIE Vol. 6908, 69080M*, 2008
- [4] L. Marigo-Lombart, S. Calvez, A. Arnoult, H. Thienpont, G. Almuneau and K. Panajotov, "Vertical electro-absorption modulator design and its integration in a VCSEL", *J. Phys. D: Appl. Phys.* 51, 2018
- [5] X. Buet, A. Guelmami, A. Monmayrant, S. Calvez, C. Tourte, F. Lozes-Dupuy, and O. Gauthier-Lafaye, "Wavelength-stabilised external-cavity laser diode using cavity resonator integrated guided mode filter", *Electronics Letters*, 48(25), 1619-1621, 2012
- [6] D. M. Pozar, *Microwave Engineering*, 4th ed. New York, NY, USA: Wiley, 2011.